Article

Cell Reports

VPS35 Deficiency or Mutation Causes Dopaminergic Neuronal Loss by Impairing Mitochondrial Fusion and Function

Graphical Abstract

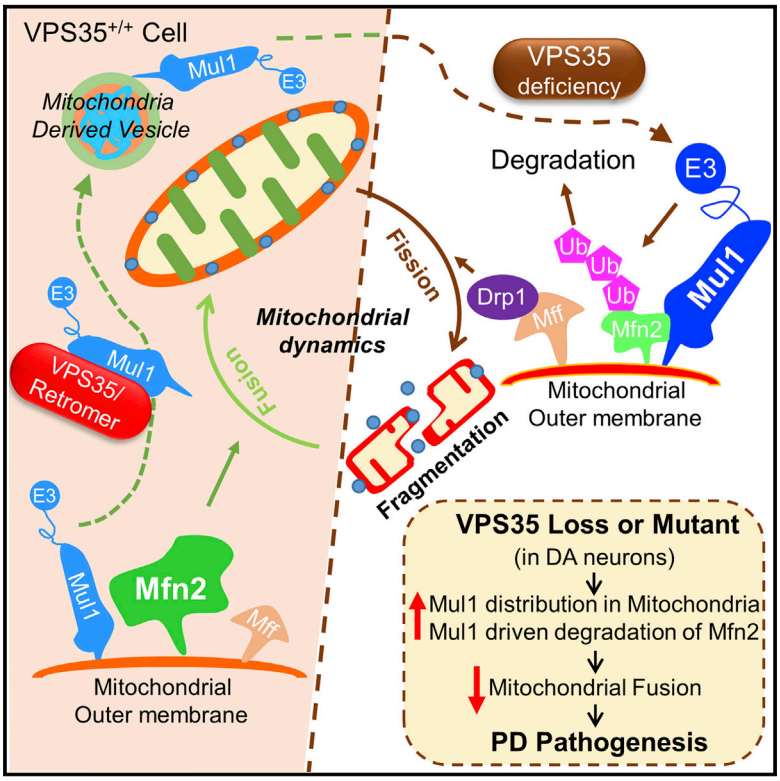

Highlights

- Genetic deletion of VPS35 in dopamine neurons results in PD-relevant pathology
- VPS35 deficiency or mutation impairs mitochondrial fusion and function
- VPS35 deficiency or mutation increases MUL1-mediated MFN2 degradation
- Mul1 suppression in DA neurons ameliorates VPS35 deficiency-induced neuronal loss

Authors

Fu-Lei Tang, Wei Liu, Jin-Xia Hu, ..., Jian Ye, Lin Mei, Wen-Cheng Xiong

Correspondence

wxiong@gru.edu

In Brief

Tang et al. find that VPS35 in mouse dopaminergic neurons is required for preventing dopaminergic neuronal loss. The function of VPS35 on dopamine neuronal survival is likely due to VPS35 promotion of MUL1 degradation, thus increasing MFN2 protein stability and mitochondrial fusion.

Tang et al., 2015, Cell Reports *12*, 1631–1643
September 8, 2015
http://dx.doi.org/10.1016/j.celrep.2015.08.001

Cell Reports
Article

VPS35 Deficiency or Mutation Causes Dopaminergic Neuronal Loss by Impairing Mitochondrial Fusion and Function

Fu-Lei Tang,[1,2] Wei Liu,[1,3] Jin-Xia Hu,[4] Joanna Ruth Erion,[1] Jian Ye,[3] Lin Mei,[1] and Wen-Cheng Xiong[1,2,*]
[1]Department of Neuroscience & Regenerative Medicine and Department of Neurology, Medical College of Georgia, Georgia Regents University, Augusta, GA 30912, USA
[2]Charlie Norwood VA Medical Center, Augusta, GA 30912, USA
[3]Department of Ophthalmology and Institute of Surgery Research, Daping Hospital, Third Military Medical University, Shapingba, Chong-Qing 400042, China
[4]Institute of Nervous System Diseases, Xuzhou Medical College, Xuzhou, Jiangsu 221002, China
*Correspondence: wxiong@gru.edu
http://dx.doi.org/10.1016/j.celrep.2015.08.001

SUMMARY

Vacuolar protein sorting-35 (VPS35) is a retromer component for endosomal trafficking. Mutations of VPS35 have been linked to familial Parkinson's disease (PD). Here, we show that specific deletion of the VPS35 gene in dopamine (DA) neurons resulted in PD-like deficits, including loss of DA neurons and accumulation of α-synuclein. Intriguingly, mitochondria became fragmented and dysfunctional in VPS35-deficient DA neurons, phenotypes that could be restored by expressing VPS35 wild-type, but not PD-linked mutant. Concomitantly, VPS35 deficiency or mutation increased mitochondrial E3 ubiquitin ligase 1 (MUL1) and, thus, led to mitofusin 2 (MFN2) degradation and mitochondrial fragmentation. Suppression of MUL1 expression ameliorated MFN2 reduction and DA neuron loss but not α-synuclein accumulation. These results provide a cellular mechanism for VPS35 dysfunction in mitochondrial impairment and PD pathogenesis.

INTRODUCTION

Vacuolar protein sorting 35 (VPS35, also called Park17) is a key component of the cargo-selective retromer complex that consists of VPS35, VPS29, and VPS26. This retromer complex sorts cargos into tubules for retrieval to the Golgi apparatus or to the cell surface (Seaman, 2012). Prominent retromer cargos include the following: the cation-independent mannose 6-phosphate receptor (CI-MPR) (Seaman, 2004), the iron transporter DMT1-II (Tabuchi et al., 2010), the Wnt transport protein Wntless (Eaton, 2008), and the sortilin-related receptor SorLA (Nielsen et al., 2007). Dysfunction of VPS35/retromer is a risk factor for both Alzheimer's disease (AD) and Parkinson's disease (PD) pathogenesis (Muhammad et al., 2008; Small et al., 2005; Small and Petsko, 2015). VPS35 is reduced in the hippocampus (HIP) of late-onset AD patients (Small et al., 2005). VPps35 haploinsufficiency enhances AD-like neuropathology in the Tg2576 mouse model of AD (Wen et al., 2011). Suppressing VPS35 expression in neonatal hippocampal neurons results in degenerative-like morphology, including abnormal dendritic spines and swollen axons (Wang et al., 2012). Intriguingly, VPS35 mutations have been identified in autosomal-dominant PD patients (Vilariño-Güell et al., 2011; Zimprich et al., 2011), and VPS35 also is reduced in the substantia nigra of PD patients (MacLeod et al., 2013). However, it remains unclear whether and how VPS35 deficiency or mutation contributes to PD pathogenesis.

Dysfunctional mitochondrial fusion/fission dynamics are believed to be a culprit for neurodegenerative disorders, including AD and PD (Knott et al., 2008). Interestingly, several genes identified in PD patients encode proteins important for mitochondrial fusion/fission dynamics, including mutations in α-synuclein (also called Park1) and leucine-rich repeat kinase 2 (Lrrk2) (Park8) that cause autosomal-dominant PD and mutations in parkin (Park2), DJ-1 (Park7), Pink1 (Park6), and ATP13A2, which have been linked to autosomal-recessive PD (Gasser, 2007; Lee et al., 2012a; Martin et al., 2011; Savitt et al., 2006; von Coelln et al., 2006). Whereas these studies have pointed to the impaired mitochondrial fusion/fission dynamics as a pathophysiological mechanism for both familial and sporadic PD, the underlying molecular mechanisms of mitochondrial fusion/fission and the relationship between dysfunctional mitochondrial fusion/fission and PD pathogenesis remain to be further explored.

The fusion/fission dynamics of mitochondria are critical not only for controlling mitochondrial shape, size, and number, but also for regulating mitochondrial functions (such as respiration and cell death/survival), clearance (e.g., mitophage), and distribution. Fission facilitates the distribution of mitochondria in response to local demand for ATP, whereas fusion helps to replace damaged mtDNA (Chan, 2006b; Karbowski and Youle, 2003). The fusion/fission dynamics are controlled by opposing actions of different dynamin-family members, such as dynamin-related protein 1 (Drp1) and mitofusins (Mfns) (Chan, 2006a; Itoh et al., 2013; Okamoto and Shaw, 2005). Fission requires Drp1 and its targeting to

mitochondria via outer membrane binding partners, including mitochondrial fission factor (Mff) (Losón et al., 2013). The activity of Drp1 is regulated by post-translational modifications, including phosphorylation, SUMOylation, and ubiquitination (Westermann, 2010). On the other hand, fusion requires mitochondrial outer membrane proteins Mfns, including Mfn1 and MFN2. Both Mfns are subjected to ubiquitination and proteasomal degradation, and MFN2 is highly expressed in the brain and implicated in Charcot-Marie-Tooth type 2A, an axonal degenerative disorder (Züchner et al., 2004).

In this paper, we provide evidence linking VPS35 deficiency and mutation to mitochondrial impairments and dopaminergic neuronal loss. VPS35 deficiency or mutation impairs mitochondrial fusion and function in cultured dopamine (DA) neurons, neuroblastoma cell lines (SH-SY5Y and NLT), and in the ventral midbrain (VM). Additionally, we show that VPS35 regulates mitochondrial fusion by promoting mitochondrial E3 ubiquitin ligase 1 (MUL1) degradation and increasing MFN2 protein stability. Suppression of MUL1 expression in VPS35-deficient DA neurons in culture and in the VM restored the PD-relevant deficits, including MFN2 decrease, mitochondrial fragmentation, and dopaminergic neuronal loss but not the increase of α-synuclein. Taken together, our results suggest that VPS35 is a critical regulator for MUL1 trafficking and degradation, thus increasing MFN2 and promoting MFN2-mediated mitochondrial fusion and DA neuron survival. Dysregulation of VPS35/retromer (due to deficiency or VPS35 mutation) impairs MUL1 degradation and mitochondrial fusion, which may underlie PD pathogenesis.

RESULTS

PD-Relevant Pathology in VPS35$^{+/-}$ Mice and in Mice with Specific Depletion of VPS35 in DA Neurons

Null-allele VPS35 mutant mice (VPS35$^{-/-}$) die early during embryonic development (Wen et al., 2011). To address whether VPS35 deficiency contributes to PD pathogenesis, we used two other mouse models, VPS35 heterozygotes (VPS35$^{+/-}$) and a newly generated mouse model with specific deletion of VPS35 gene in DA neurons (VPS35$^{DAT\text{-}Cre}$). The VPS35$^{+/-}$ mice survived to adult age without a defect in lifespan (Wen et al., 2011). Before the age of 6 months old, the PD-relevant deficits, such as the loss of DA neurons and increase of α-synuclein, were not obviously detected in VPS35$^{+/-}$ mice (Tang et al., 2015). However, at 12 months old, ~20% of DA neuron loss was detected in the SNpc of VPS35$^{+/-}$ brain compared with that of VPS35$^{+/+}$ controls, and VPS35$^{+/-}$ mice showed an increase in α-synuclein levels in the VM, too (Tang et al., 2015). These results demonstrate that VPS35$^{+/-}$ mice display an age-dependent DA neuron loss and accumulation of α-synuclein, both pathological features of PD, suggesting that VPS35 haploinsufficiency promotes PD pathogenesis.

VPS35 is expressed in multiple cell types in the brain, including DA neurons (MacLeod et al., 2013) and glial cells (data not shown). To address if VPS35 expression in DA neurons is essential for the prevention of PD-like deficits, we generated VPS35$^{DAT\text{-}Cre}$ mice by crossing floxed VPS35 (VPS35$^{f/f}$) with DAT-Cre mice (Figures S1A–S1C), where Cre recombinase is under the control of the promoter of DA transporter gene (DAT) and specifically expressed in DA neurons (Figure S1C; Zhuang et al., 2005). Thus, the VPS35 protein was specifically depleted in SNpc-DA neurons (Figure S1D). The VPS35$^{DAT\text{-}Cre}$ mice survived to adult age (up to 6 months of age examined) with a slight reduction in body weight and size (Figure S1E). Remarkably, at young adult age (2–3 months old), VPS35$^{DAT\text{-}Cre}$ mice showed a marked reduction in TH$^+$ DA neurons at the SNpc and a decrease in TH$^+$ fibers in striatum (STR), compared with those of littermate controls (VPS35$^{f/f}$) (Figures 1A–1D). The neuronal loss in SNpc of VPS35$^{DAT\text{-}Cre}$ mice was confirmed by NeuN staining analysis (Figures 1A and 1B). The reduction of TH proteins was further verified by western blot analysis (Figures 1E and 1F). In addition, increased α-synuclein levels were detected in the VM/SNpc-DA neurons of VPS35$^{DAT\text{-}Cre}$ mice (Figures 1E–1H). Furthermore, we examined if VPS35$^{DAT\text{-}Cre}$ mice showed PD-relevant motor deficit. In the automatic gait test, VPS35$^{DAT\text{-}Cre}$ mice displayed significant unsteady and weaker gaits (Figure 1I). VPS35$^{DAT\text{-}Cre}$ mice also exhibited a decline in hindlimb stepping (rearing behavior) in the cylinder observational test (Figure 1J), and they took more time to descend the pole by the vertical pole test (Figure 1K). In the open-field test, VPS35$^{DAT\text{-}Cre}$ mice showed a significant reduction in the overall locomotor activity, including shorter total distance traveled and increased immobile time (Figure 1L). These results indicate that VPS35$^{DAT\text{-}Cre}$ mice exhibit reduced locomotor activity.

Taken together, these results demonstrate that VPS35$^{DAT\text{-}Cre}$ mice exhibit earlier onset of PD-relevant pathological features than that of VPS35$^{+/-}$ mice, revealing the necessity of VPS35 expression in DA neurons for the prevention of PD pathogenesis.

Reduced Mitochondrial MFN2 in VPS35-Deficient DA Neurons

To understand how VPS35 in DA neurons prevents PD pathogenesis, we examined whether VPS35 deficiency altered levels of proteins critical for endosomes (EEA1), Golgi (GM130), lysosomes (LAMP1), mitochondrial fission/fusion (Drp1 and MFN2), mitochondria (Tom20), and proteins implicated in PD pathogenesis, such as Lrrk2, Pink1, and Parkin. Homogenates prepared from various brain regions, including VM, HIP, and STR, of control (VPS35$^{f/f}$) and VPS35$^{DAT\text{-}Cre}$ mice were subjected to western blotting analyses. As shown in Figures 2A and 2B, no obvious change was observed for EEA1, GM130, LAMP1, Lrrk2, Pink1, Parkin, Tom20, and Drp1. However, MFN2 was significantly reduced in the VM, but not the HIP or STR regions, of VPS35$^{DAT\text{-}Cre}$ mice (Figures 2A and 2B). MFN2 is a GTPase embedded in the outer membrane of the mitochondria (Chen et al., 2003).

We thus examined if mitochondrial MFN2 is reduced in VPS35-deficient brain. Mitochondrial fractions were purified from the VM region of control and VPS35$^{+/-}$ mice at different ages and subjected to western blotting. MFN2 was reduced in VPS35$^{+/-}$ VM mitochondria, whereas no obvious change was observed for Lrrk2, Pink1, Parkin, ATP5a, Tom20, and Drp1, even in aged mutant mice (Figures 2C and 2D). We next examined if mitochondrial MFN2 is reduced in VPS35-deficient neurons in culture. Indeed, a marked MFN2 reduction in Mito-RFP-labeled mitochondria was detected in neurons expressing microRNA (miRNA)-VPS35, which reduced VPS35 by >80%

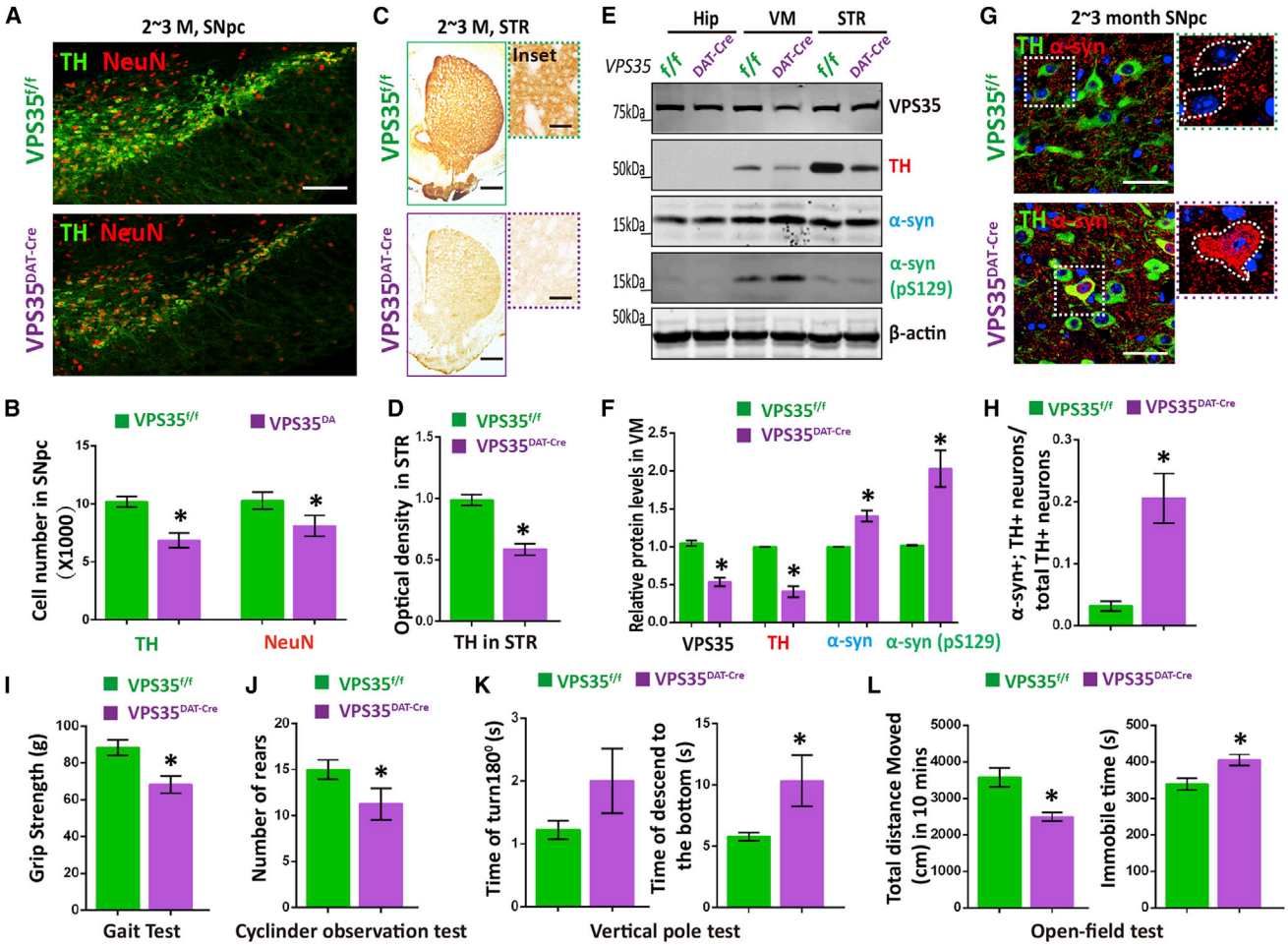

Figure 1. PD-Relevant Neuropathology in VPS35$^{DAT-Cre}$ Mice

(A and B) Loss of TH$^+$-DA neurons in 2- to 3-month-old VPS35$^{DAT-Cre}$ SNpc. (A) Representative images of midbrain coronal sections of VPS35$^{DAT-Cre}$ and $^{f/f}$ littermates are shown (scale bars represent 200 μm). (B) Data were quantified by stereological analysis total numbers of TH$^+$ or NeuN$^+$ cells in SNpc and are shown as mean ± SEM (n = 4; *p < 0.05).

(C and D) Immunostaining analysis showing reduced TH$^+$ neuronal processes in 2- to 3-month-old VPS35$^{DAT-Cre}$ STR. (C) Representative images of the whole STR are shown (scale bars represent 400 μm). (Inset) Close-up views of neuronal processes are shown (scale bars represent 10 μm). (D) Quantification of TH optical density is shown (mean ± SEM; n = 4; *p < 0.05).

(E and F) Western blot analysis of TH and α-synuclein (α-syn) levels from ventral midbrain (VM) of 2- to 3-month-old VPS35$^{DAT-Cre}$ and VPS35$^{f/f}$ mice. Data were quantified and are presented in (F) as mean ± SEM (n = 4; *p < 0.05).

(G and H) Accumulation of α-syn in VPS35$^{DAT-Cre}$ SNpc-DA neurons. Midbrain coronal sections of indicated mice were immunostained with α-syn (red) and TH (green) antibodies. (G) Representative images are shown (scale bar represents 10 μm). (H) Quantitative data of α-syn somatic accumulation in TH$^+$ neurons (%, over total TH$^+$ neurons) in SNpc are presented (mean ± SEM; n = 4; *p < 0.01).

(I–L) Behavioral tests on VPS35$^{DAT-Cre}$ mice and control littermates. (I) Grip strength: forelimb grip strength was determined by a digital weight gauge. (J) Cylinder observational test: rearing frequency was recorded. (K) Pole test: each mouse was placed head upward on a round vertical pole and performance was determined by the latency(s) of the mouse to turn downward and completely descend the pole. (L) Open-field tests: total distance traveled and immobile time in open-field test were quantified in (E). Data are presented as mean ± SEM (n = 4–6; *p < 0.05).

(Wang et al., 2012; Figures 2E and 2F). MFN2 reduction also was confirmed by western blot analysis of lysates of cultured DA neurons from VPS35$^{DAT-Cre}$ mice (Figures 2G and 2H). A similar MFN2 reduction was detected in small hairpin RNA (shRNA)-VPS35-expressing SH-SY5Y and NLT cells by both western blot and immunostaining analyses (Figure S2). Taken together, these results suggest that VPS35 deficiency in DA neurons as well as neuronal cell lines reduced mitochondrial MFN2, identifying a potential molecular target.

Mitochondrial Fragmentation in VPS35$^{DAT-Cre}$ DA Neurons and Neurons Expressing PD-Linked VPS35 Mutant

MFN2 is essential for mitochondrial fusion (Chen et al., 2003), which is frequently altered by PD-linked genetic mutations (Haelterman et al., 2014). We thus examined mitochondrial morphology in VPS35-deficient DA neurons. Overall, VPS35$^{DAT-Cre}$ DA neurons (TH$^+$) in culture showed no obvious defect in neuronal processes (revealed by TH and Tuj1 staining) (Figure 3A; data not

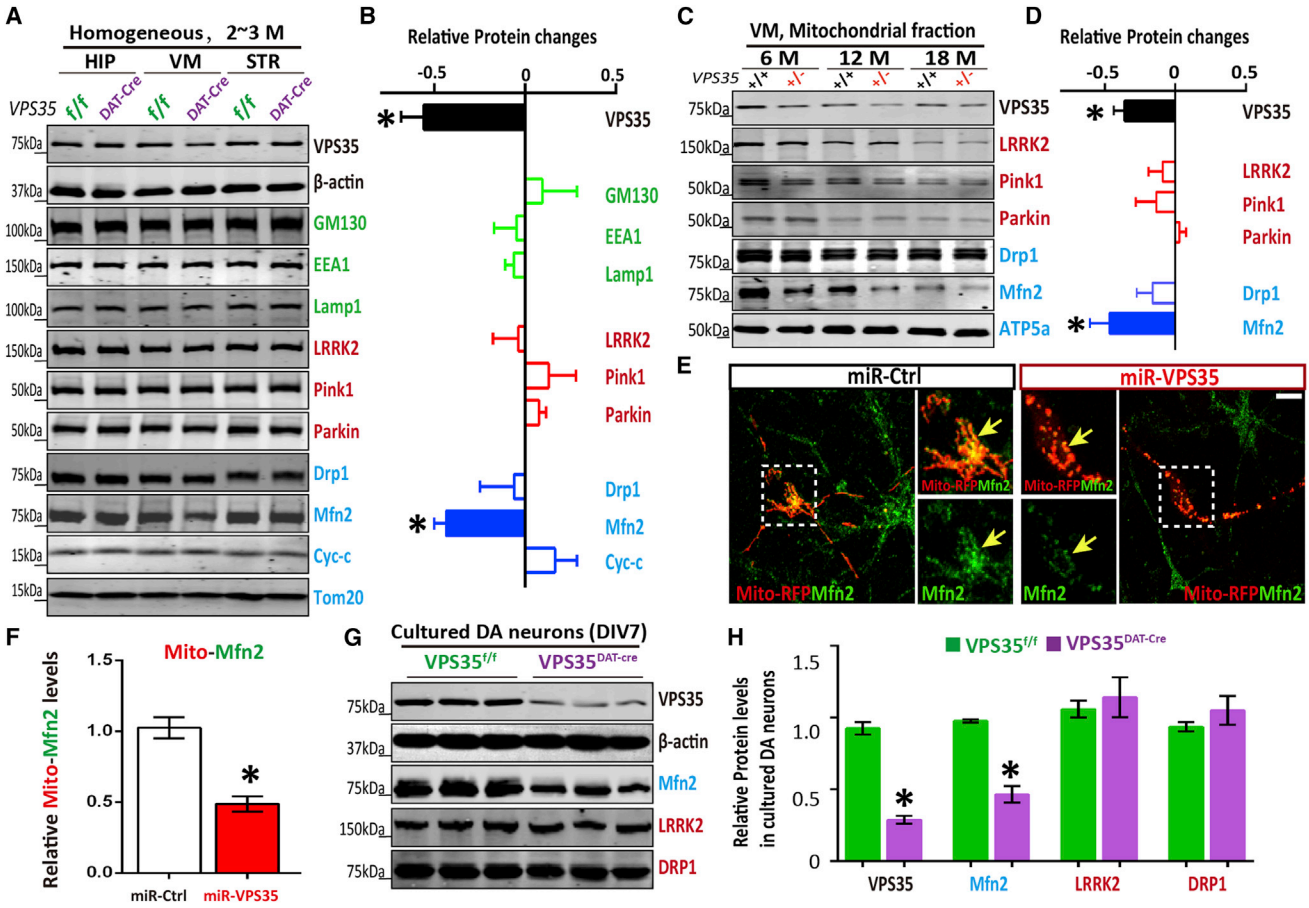

Figure 2. Reduced Mitochondrial MFN2 in Vps35-Deficient DA Neurons

(A and B) Reduced MFN2 in $Vps35^{DAT\text{-}Cre}$ VM, but not hippocampus (HIP) or striatum (STR). Soluble extracts from HIP, VM, and STR of indicated mice were subjected to western bot analysis (A, representative blots; B, quantification of protein levels compared with $Vps35^{f/f}$ controls). Data are presented as mean ± SEM (n = 3 mice/genotype; *$p < 0.05$).

(C and D) Reduced mitochondrial MFN2 in aged $Vps35^{+/-}$ VM. Mitochondrial fractions of indicated mice were subjected to western bot analysis (C, representative blots; D, quantification of protein levels compared with $Vps35^{+/+}$ controls). Data are presented as mean ± SEM (n = 3 mice/genotype; *$p < 0.05$).

(E and F) Reduced mitochondrial MFN2 in miRNA-Vps35-expressing neurons. (E) Representative images of transfected neurons are shown. (F) Quantitative data (normalized by control miR) are shown (mean ± SEM; n = 5 neurons; *$p < 0.05$).

(G and H) Reduced MFN2 levels in $Vps35^{DAT\text{-}Cre}$ primary DA neurons. (G) Representative blots are shown. (H) Quantification of protein levels (normalized with $Vps35^{f/f}$ controls) is shown. Data are presented as mean ± SEM (n = 3 mice/genotype; *$p < 0.05$).

shown). However, mitochondria of VPS35-depleted DA neurons (revealed by Tom20, a marker for mitochondrial outer membrane) were shorter and rounder than those in control neurons (Figures 3A and 3B), suggesting mitochondrial fragmentation. Importantly, the mitochondrial fragmentation in VPS35-depleted neurons was mitigated by expressing GFP-fused VPS35-wild-type (WT), but not VPS35-D620N, the PD-linked VPS35 mutant (Figures 3C and 3D). These results thus reveal a cell-autonomous function of VPS35 in preventing mitochondrial fragmentation in neurons, and they provide a possible pathophysiological mechanism of the PD-linked VPS35-D620N mutation.

Note that mitochondrial fragmentation also was observed in NLT and SH-SY5Y neuronal cell lines that were transfected with miRNA-VPS35 (Figures S3A–S3D) or shRNA-VPS35 (Figures S3E–S3G). This mitochondrial fragmentation was restored by expressing shRNA-resistant, but not shRNA-sensitive, VPS35 in shRNA-VPS35-expressing NLT cells (Figures S3E–S3G). These results demonstrate that VPS35 deficiency or mutation results in mitochondrial fragmentation in DA neurons as well as neuronal cell lines.

Impaired Mitochondrial Function in VPS35-Deficient DA Neurons

Mitochondrial fusion morphology is believed to be critical for the maintenance of mitochondrial respiratory capacity in mammalian cells (Westermann, 2012). Deficits in mitochondrial respiration are critically associated with dopaminergic neuronal dysfunction in PD (Itoh et al., 2013). We thus examined mitochondrial respiratory capacity in VPS35-deficient DA neurons by use of the Seahorse platform to measure real-time oxygen (O_2) consumption rates (OCRs). The basal oxygen consumption rate (BR) was slightly higher in DA neurons from $VPS35^{DAT\text{-}Cre}$

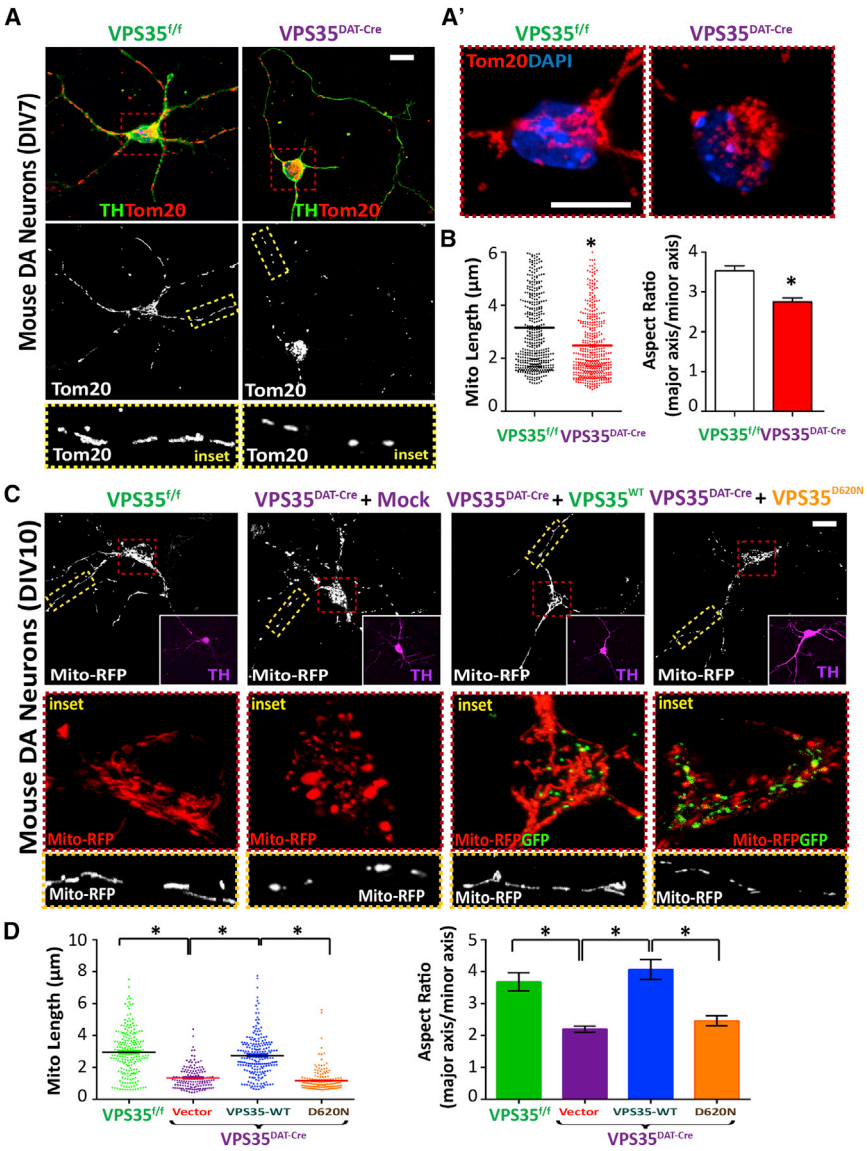

Figure 3. Mitochondrial Fragmentation in VPS35$^{DAT-Cre}$ DA Neurons

(A and B) Increased mitochondrial fragmentation in primary DA/TH+ neurons (7 DIV) from VPS35DAT-Cre midbrain, compared to VPS35$^{f/f}$ controls. Midbrain neurons of E18.5 mice were cultured for 7 days (7 DIV). Mitochondria were labeled by Tom20 staining. (A) Representative images and close-up views of mitochondria in neurites are shown. (A') Close-up views of mitochondria in neuron soma region are shown (scale bars represent 10 μm). (B) Quantifications of mitochondrial length and aspect ratio (mitochondrial major axis over minor axis) are shown. Shown are grouped column scatter (left, with mean indicated by the line) and as aspect ratio (right, presented as mean ± SEM; n = 400 mitochondria from 20 different neurons of each group; *p < 0.05).

(C and D) Reduced mitochondrial fragmentation in VPS35$^{DAT-Cre}$ DA neurons expressing VPS35-WT, but not VPS35-D620N. Primary VPS35$^{DAT-Cre}$ DA neurons were transfected with VPS35-WT-GFP or VPS35-D620N-GFP (GFP was fused with the VPS35-C terminus) at 6 DIV and analyzed for mitochondrial morphology at 10 DIV. (C) Representative images are shown (scale bars represent 10 μm). (D) Quantifications of mitochondrial length and aspect ratio are shown. Data are presented as mean ± SEM (n = 200 mitochondria from ten different neurons; *p < 0.01).

mice compared with controls, whereas no difference in oxygen consumption was observed following treatment of neurons with oligomycin (an inhibitor of ATP synthase), which serves as a negative control (Figures 4A and 4B). However, the maximal respiratory rates (MRs) induced by mitochondrial un-coupler (carbonyl cyanide-p-trifluoromethoxyphenylhydrazone [FCCP]) treatment were markedly reduced in VPS35-depleted DA neurons (Figures 4A and 4B), which resulted in a deficiency in spare respiratory capacity (SR) (Figure 4C). A similar mitochondrial MR deficit also was detected in VPS35$^{+/-}$ DA neurons (data not shown). These results thus indicate dysfunctional mitochondria in cultured VPS35-deficient DA neurons.

Mitochondrial membrane potential (Ψm) is another indicator of mitochondrial health and function (Chen, 1988). We then asked if VPS35 deficiency alters mitochondrial membrane potential by using the potentiometric fluorescent dye tetramethylrhodamine methylester (TMRM), as its fluorescent intensity reflects the mitochondrial membrane potential. NLT, a GnRH neuronblastoma cell line, was used because VPS35 is highly expressed in NLT cells (Wen et al., 2011) and the spread cell morphology in NLT cells provides a technical advantage for this assay. As shown in Figures 4D and 4E, TMRM accumulated in control NLT cells and the fluorescence was decreased by treatment with carbonyl cyanide m-chlorophenyl hydrazine (CCCP), a proton ionophore that depolarizes mitochondria, indicating the specificity of TMRM labeling. However, TMRM signal was reduced in miRNA-VPS35-expressing cells, which agrees with the increased respiratory rate in OCR test (Figures 4D–4F). Taken together, these results suggest that mitochondrial dysfunction occurs in VPS35-deficient DA neurons as well as NLT cells.

In Vivo Mitochondrial Deficit in VPS35-Deficient Midbrain

To determine whether mitochondrial structures were altered in VPS35-deficient brain, we carried out transmission electron microscopy (TEM) analysis. As shown in Figures S4A–S4D, mitochondria were smaller in VPS35$^{+/-}$ SNpcs in 4-month-old mice. The deficit was undetectable in STR of the mutant mice, but became prominent in 12-month-old mutant mice (Figures S4B, S4C, and S4E). The STR mitochondria in 12-month-old mutant mice were condensed and damaged (Figure S4F). These results

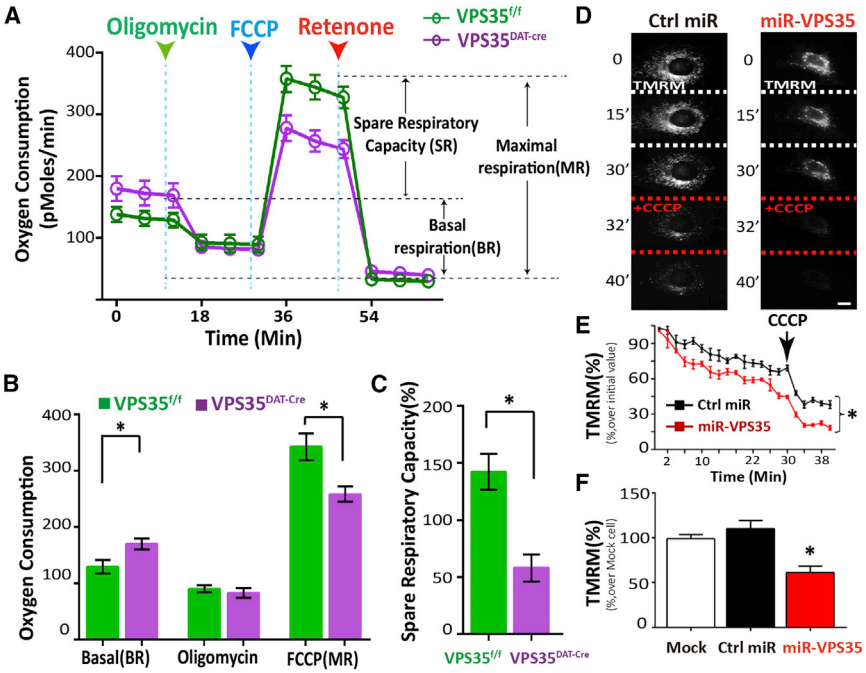

Figure 4. Impaired Mitochonchrial Function in VPS35$^{DAT-Cre}$ DA Neurons and VPS35-Deficient NLT Cells

(A and B) Real-time O_2 consumption rate (OCR) was measured in 7 DIV primary DA neurons by a Seahorse XF96 analyzer. For validation of the measurement, we used the ATP synthase inhibitor oligomycin (2 μM) after recording basal line, followed by treatments of the pharmaceutical uncoupler FCCP (3 μM) and the complex I inhibitor rotenone (1 μM). Representative traces of OCR are indicated in (A), each time point representing the mean ± SEM, and averaged OCR profiles from at least four animals are shown in (B). *$p < 0.05$.

(C) The SR changes (compared with BR) are shown with bar graph. Data are presented as mean ± SEM (*$p < 0.01$).

(D–F) Decreased mitochondrial membrane potential in miRNA-VPS35-expressing NLT cells. (D) Representative TMRM time-lapse images of transfected NLT cells, without or with 20 μM CCCP, are shown (scale bar represents 10 μm). (E) Quantitative data are shown. Arrow indicates CCCP treatment. (F) ΔΨm in NLT cells expressing control or miR-VPS35 is shown (mean ± SEM; n = 50 cells; *$p < 0.01$).

thus indicate that mitochondria appear to be fragmented and abnormal in morphology in aged VPS35$^{+/-}$ midbrains and STRs, which may underlie PD-relevant neuropathology.

To ascertain if mitochondria in VPS35$^{+/-}$ brain are dysfunctional, we measured mtDNAs, which are largely dependent on fusion and have been used as an indicator of mitochondrial function (Chan, 2006a). The ratio of mtDNAs over nuclear DNAs (ncDNAs) in VM and STR was similar between VPS35$^{+/+}$ and VPS35$^{+/-}$ mice at 3 months of age (Figure S4G). However, the ratio was markedly decreased in 12-month-old VPS35$^{+/-}$ VM and STR, compared with that of WT controls (Figure S4G, bottom). This effect was not observed in the HIP, indicating regional specificity. These results provide additional evidence for age-dependent and brain region-specific mitochondrial dysfunction.

MFN2 Protein Reduction Associated with Increased Ubiquitination

We then investigated the underlying molecular mechanisms for MFN2 reduction in VPS35-deficient brain/neurons. The MFN2 reduction was not caused by a problem in transcription, because a comparable level of MFN2 mRNA was detected between control and mutant mice (Figure S2E). MFN2 can be degraded by the ubiquitin-proteasome system (UPS) (Tanaka et al., 2010). We thus speculated that the MFN2 reduction might be due to MFN2 degradation by the UPS. This notion was supported by the observation that MG132, a proteasome inhibitor, restored MFN2 levels in VPS35-deficient DA neurons (Figures S5A and S5B) or SH-SY5Y cells (Figures S5C and S5D). Consistently, MFN2 ubiquitination was increased in VPS35-deficient SH-SY5Y cells or cells expressing VPS35 mutant (D620N) (Figures S5E and S5F). Interestingly, expression of shRNA-resistant VPS35-WT, but not VPS35-D620N, also restored MFN2 levels in VPS35-deficient SH-SY5Y cells (Figures S5C and S5D). These results suggest that VPS35 deficiency or mutation (D620N) reduces MFN2 protein likely by UPS-mediated MFN2 degradation.

Increase of Mitochondrial E3 Ubiquitin Ligase MUL1

A previous proteomic study suggested that MUL1 (also known as MAPL for mitochondrial-anchored protein ligase) interacts with VPS35/retromer (Braschi et al., 2010). Recently, MUL1, a mitochondrial outer membrane protein, was found to be a critical E3 ubiquitin ligase of MFN2 (Lokireddy et al., 2012). To determine if MUL1 was involved in VPS35 regulation of MFN2, we examined MUL1 protein levels in mitochondrial fractions of different brain regions of control and mutant mice (at 4 months old). MUL1 levels were selectively elevated in mitochondrial fractions of VPS35$^{+/-}$ VMs and STRs, but not HIP, corroborating with MFN2 reduction (Figures 5A and 5B). In VPS35-deficient SH-SY5Y cells, a MUL1 increase was also detectable, which was associated with a decrease in MFN2 (Figures 5C and 5D), revealing a reciprocal relationship between MUL1 and MFN2 that suggests MFN2 as an MUL1 substrate. Additionally, the MUL1 increase was mitigated by co-expressing shRNA-resistant VPS35-WT but not VPS35-D620N (Figures 5C and 5D). Finally, expression of this and other PD-associated mutants (P316S or R524W) was sufficient to increase MUL1 and reduce MFN2 (Figures 5E and 5F). These results suggest that VPS35 regulates MUL1 protein level, which may be involved in VPS35 deficiency-induced MFN2 reduction.

To understand how VPS35 regulates MUL1 protein level, we measured the half-life of MUL1 in control and shRNA-VPS35-expressing SH-SY5Y cells. The half-life of MUL1 in control cells was about 4 hr (Figures 6A and 6B). However, it dramatically increased in shRNA-VPS35-expressing cells, with no detectable

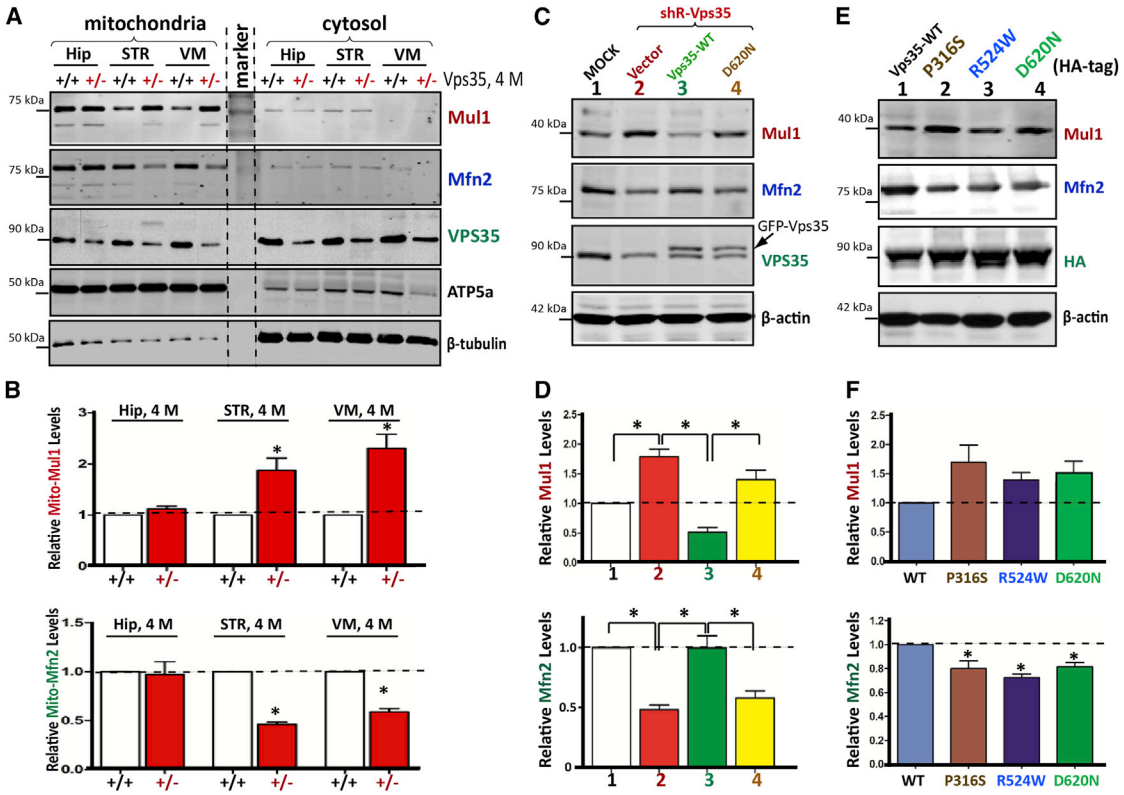

Figure 5. Increased MUL1 in VPS35$^{+/-}$ Midbrains and in SH-SY5Y Cells Expressing shRNA-VPS35 or PD-Linked VPS35 Mutants

(A and B) Increased mitochondrial-MUL1 protein in 4-month-old VPS35$^{+/-}$ VM and STR, but not HIP. Mitochondrial fractions were subjected to western blotting with the indicated antibodies. (A) Representative blots are shown. (B) Quantification of data (normalized by VPS35$^{+/+}$ control) is shown.

(C and D) Association of increased MUL1 with decreased MFN2 in shRNA-VPS35-expressing SH-SY5Y cells, which was restored by expressing shRNA-resistant VPS35-WT, but not VPS35-D620N. (C) Representative blots are shown. (D) Quantification of MUL1 and MFN2 protein (normalized by Mock control) is shown.

(E and F) Association of increased MUL1 with decreased MFN2 in SH-SY5Y cells expressing PD-linked VPS35 mutants. (E) Representative blots are shown. (F) Quantification of MUL1 and MFN2 protein levels (normalized by VPS35-WT control) is shown. Data in (B), (D), and (F) are presented as mean ± SEM (n = 3; *p < 0.05).

reduction within 8 hr of experiments (Figures 6A and 6B). These results indicate that VPS35 is necessary for MUL1 degradation. To determine if MUL1 distribution in mitochondria was altered in VPS35-deficient cells, we stained for MUL1 in miRNA-VPS35-expressing NLT cells and VPS35$^{+/-}$ neurons. As shown in Figures 6C–6E, exogenous MUL1 (GFP-MUL1) and endogenous MUL1 in mitochondria were markedly increased in VPS35-deficient NLT and neurons, compared to those in control cells. The increase of mitochondrial-MUL1 in VPS35$^{+/-}$ neurons also was ameliorated by expressing VPS35-WT, but not VPS35-D620N (Figures 6F and 6G). These results were in agreement with increased MUL1 in mitochondrial fractions of VPS35$^{+/-}$ VMs (Figures 5A and 5B). These results led us to propose that VPS35 promotes the degradation of MUL1 to reduce MUL1 level in mitochondria, which may be critical for maintaining MFN2 protein level for mitochondrial fusion.

Requirement of MUL1 for MFN2 Reduction, Mitochondrial Fragmentation, and DA Neuron Loss in VPS35-Deficient Cells or Midbrain

To investigate whether MUL1 is involved in MFN2 reduction in VPS35-deficient cells, we generated shRNA-MUL1 (shR-MUL1), which specifically and efficiently suppressed MUL1 expression (Figures S6A–S6C). As shown in Figures S6A and S6B, co-expressing shR-MUL1 prevented miRNA-VPS35 from reducing MFN2 in SH-SY5Y cells. Moreover, shR-MUL1 prevented VPS35 deficiency from causing mitochondrial fragmentation in either miRNA-VPS35-expressing NLT cells (Figures S6D and S6E) or neurons (Figures S6F and S6G). These results demonstrate that MFN2 reduction and mitochondrial fragmentation by VPS35 deficiency require MUL1, providing a molecular mechanism by which VPS35 deficiency causes MFN2 degradation and mitochondrial fragmentation.

We further tested this view by determining whether MUL1 causes MFN2 reduction in VPS35-deficient DA neurons in vivo. To this end, adenovirus (serotype 5)-encoding shRNA against mouse MUL1 (AAV-shR-MUL1-GFP) was generated, which was injected into VPS35$^{+/+}$ and VPS35$^{+/-}$ SNpc (at 6 months of age) (Figure 7A). Two months post-virus injection, GFP expression throughout the injected SNpc was observed (Figure 7B) and >80% of TH-positive neurons expressed GFP (Figure 7B, insets). As DA neurons of the SNpc project to the STR to create the nigral-striatal pathway, the GFP signal in the ipsilateral, but not contralateral (CON), STR also was detected,

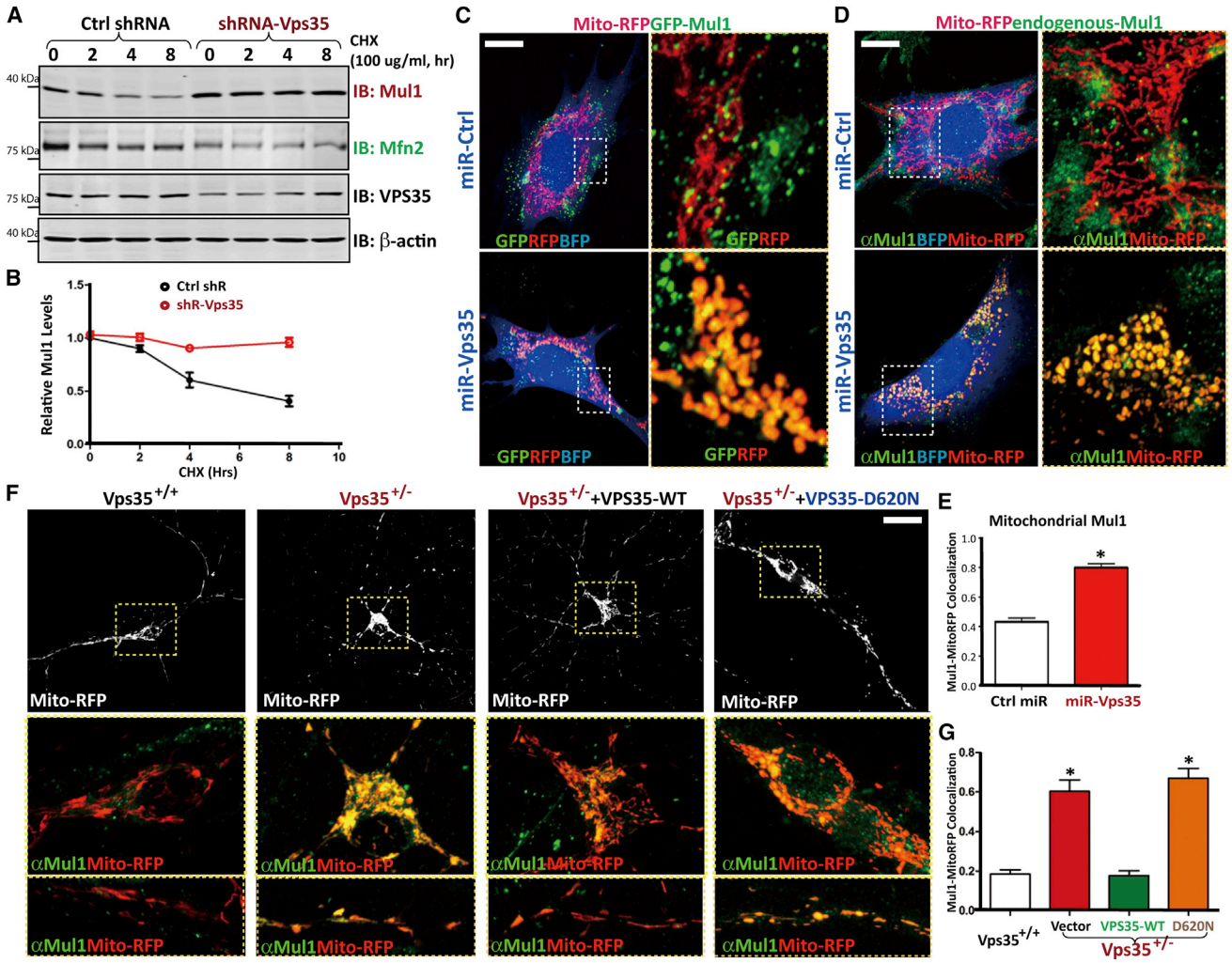

Figure 6. Impaired MUL1 Degradation and Increased MUL1 Distribution in Mitochondria in VPS35-Deficient Cells

(A and B) MUL1 protein degradation was inhibited by shRNA-VPS35. SH-SY5Y cells were transfected with control and shRNA-VPS35 (at ~80% efficiency). Transfected cells were incubated with CHX (100 mg/ml) for the indicated times. Cell lysates were subjected to western blotting using the indicated antibodies (A, representative blots; B, quantification of MUL1 levels, each time point representing the mean ± SEM normalized with time 0).

(C–E) MUL1 distribution in mitochondria was increased in miRNA-VPS35-expressing NLT cells. GFP-MUL1 (C) and endogenous MUL1 (D) were increased in mito-RFP-labeled mitochondria of miRNA-VPS35-expressing cells (C and D, representative images; scale bar represents 5 μm). MUL1 colocalization with mitochondria (Mito-RFP) is presented in (E) as mean ± SEM; n = 3, each with 20 cells; *p < 0.05.

(F and G) MUL1 distribution in mitochondria was increased in VPS35$^{+/-}$ neurons, which was reduced by GFP-VPS35-WT, but not GFP-VPS35-D620N. (F) Representative images are shown (scale bar represents 10 μm). (G) Quantification of MUL1 co-localization with mitochondria is shown (mean ± SEM; n = 3, each with 20 cells; *p < 0.05).

indicating the specificity of the injection (Figure 7B). Western blot analysis confirmed that AAV-shR-MUL1-GFP infection efficiently suppressed MUL1 expression in both WT and VPS35$^{+/-}$ VMs (Figures 7C and 7D). Remarkably, the MFN2 level was restored to normal in VPS35$^{+/-}$ VMs and increased in WT VMs by suppressing MUL1 expression (Figures 7C and 7D), indicating the necessity of MUL1 for the MFN2 reduction in vivo.

Interestingly, upon AAV-shR-MUL1-GFP injection, TH^{+} neuron counts in VPS35$^{+/-}$ SNpc were restored to a nearly normal range (Figures 7E and 7F). The TH^{+} neurons in the CON side of VPS35$^{+/-}$ SNpc remained lower than that of VPS35$^{+/+}$ controls (Figures 7E and 7F), indicating the specificity. Consistently, TH protein was reduced in VPS35$^{+/-}$ VMs, which was restored by infection with the virus of AAV-shR-MUL1-GFP (Figure 7C). TH^{+} dopaminergic nerve terminals also were decreased in VPS35$^{+/-}$ STR compared with those of WT controls, which also were rescued by suppressing MUL1 expression (Figures 7G and 7H). We further measured DA neurotransmitter level by high-performance liquid chromatography (HPLC) in VPS35$^{+/+}$ and VPS35$^{+/-}$ STR injected with or without the shR-MUL1-GFP virus. Whereas DA was markedly reduced in VPS35$^{+/-}$ STR (compared with that of WT controls), suppressing MUL1 expression prevented this DA reduction (Figure 7I). It is noteworthy that the increase of α-synuclein in VPS35$^{+/-}$ VM was

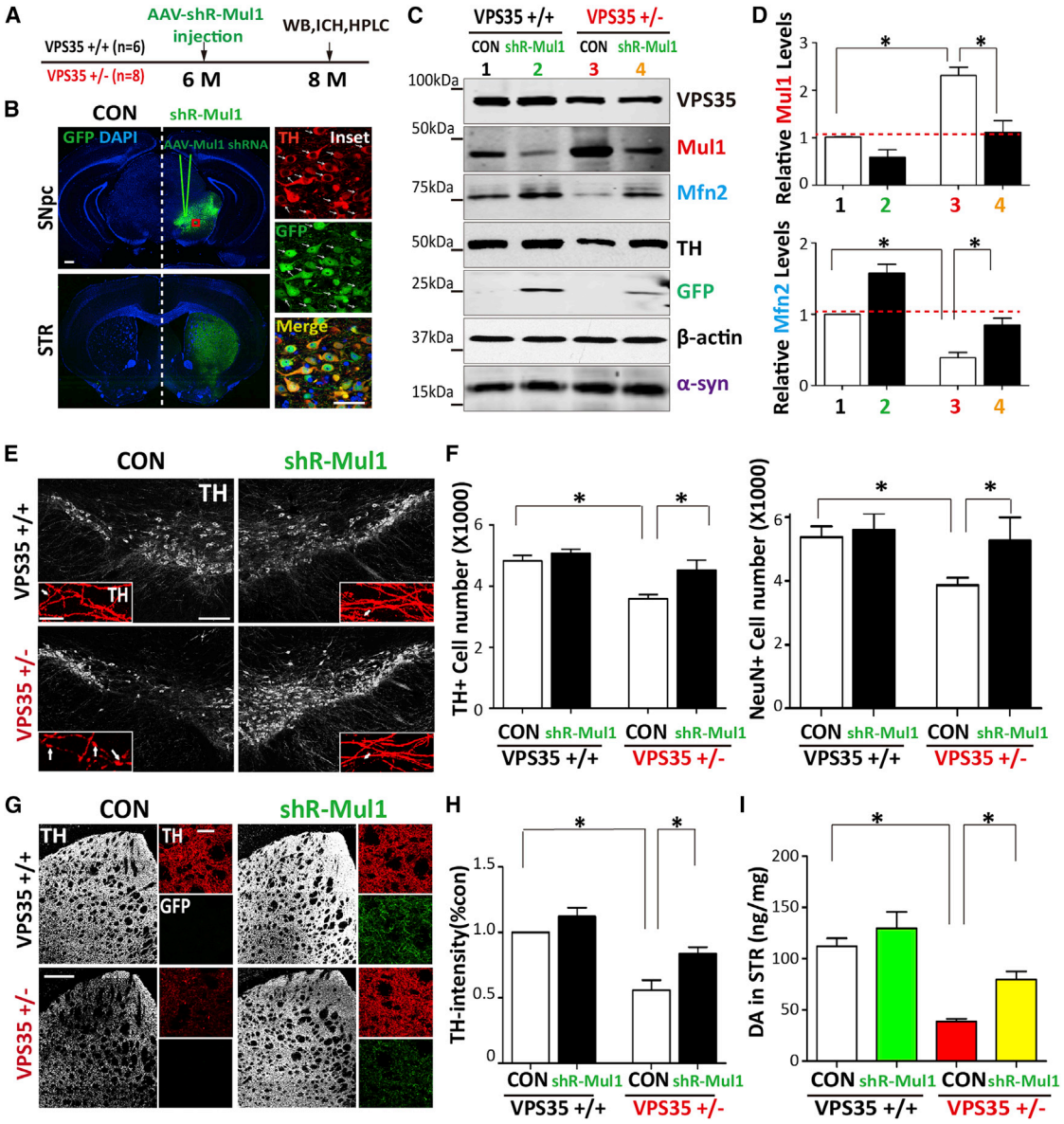

Figure 7. Restoration of MFN2 Reduction and DA Neuron Loss by Suppressing MUL1 Expression in VPS35$^{+/-}$ SNpc

(A) Schematic of AAV injection strategy. AAV5-shR-MUL1-GFP was stereotactically injected into VPS35$^{+/+}$ or Vps$^{+/-}$ mice brains at 6 months of age. Two months post-injection, coronal brain sections, VMhomogenates, or STR homogenates were collected and subjected to immunohistochemical staining, western blot, and HPLC analysis.

(B) AVV5 infect the DA neurons in coronal brain sections. Contralateral (CON) and ipsilateral (shR-MUL1) substantia nigra (SNpc) are indicated (scale bar represents 1mm). Right insets show magnified images of the marked squares (scale bar represents 50 μm).

(C) Representative western blots of homogenates of VM derived from the virus ipsilateral (shR-MUL1) and CON hemispheres.

(D) Quantification of data from (C). Relative MUL1 and MFN2 protein levels were normalized by un-injection side of VPS35$^{+/+}$. Means ± SEM (n = 3) are shown; *p < 0.05.

(E and F) Stereological analysis of TH-positive dopaminergic neurons in the SNpc. (E) Representative images show TH immunostaining analysis in the virus-injected SNpc (scale bar represents 200 μm). Insets show magnified images (scale bar represents 10 μm) and arrows indicate axon swelling. Quantification analysis of TH^{+} or NeurN^{+} cells in each hemisphere (mean ± SEM; n = 3) are presented in (F). *p < 0.05 by one-way ANOVA with post hoc analysis.

(G and H) Distribution of TH-immunoreactive fibers in the STR. (G) Representative images of TH staining analysis in adjacent sections of the injected STR (scale bar represents 400 μm). Insets show magnified images (scale bar represents 10 μm). (H) Quantification of TH-immunoreactive intensity in the STR. Data are expressed as the percentage of the TH intensity of VPS35$^{+/+}$ CON side. Mean ± SEM; n = 3; *p < 0.05 by one-way ANOVA with post hoc analysis.

(I) Dopamine levels in the VPS35$^{+/+}$ and VPS35$^{+/-}$ STR were measured by HPLC analysis. Isoproterenol was added as internal control (n = 3). Data are presented as mean ± SEM; *p < 0.05 by one-way ANOVA with post hoc analysis.

unchanged by suppression of MUL1 expression (Figure 7C). Collectively, these findings suggest that VPS35 deficiency reduces MFN2 and promotes dopaminergic neuronal loss, which can be alleviated by suppression of MUL1 expression.

Next, we determined whether MUL1 also causes MFN2 reduction in DA neurons expressing PD-linked VPS35 mutant (D620N) in vivo. To this end, AAV5-encoding GFP-T2A-VPS35-D620N was generated, which was injected or co-injected with shR-MUL1 virus into WT-SNpc (at 3 months old) (Figure S7A). Western blot and immunostaining analysis confirmed the VPS35-D620N expression and the MUL1 suppression by infecting WT VM with both viruses (Figures S7B–S7D). Indeed, MFN2 was reduced in VMs expressing VPS35-D620N, which was restored to normal in VMs co-expressing shRNA-MUL1 (Figures S7B and S7C). Accordantly, the TH^+ neurons were lower in VPS35-D620N-expressing SNpc, which was attenuated by co-expression of shR-MUL1 (Figures S7G and S7H). Interestingly, in VPS35-D620N-expressing DA neurons, mitochondria were shorter and round (indicators of mitochondrial fragmentation) compared with those of uninfected or AAV-GFP-infected control neurons (Figures S7E and S7F). Moreover, co-injection with shR-MUL1 virus prevented mitochondrial fragmentation in these VPS35-D620N-expressing DA neurons (Figures S7E and S7F). Taken together, these results suggest that VPS35 mutation (D620N) acts as VPS35 deficiency, promoting dopaminergic neuronal loss likely by increasing MUL1-mediated MFN2 degradation.

DISCUSSION

This study has the following major findings. First, VPS35 expression in DA neurons is essential for prevention of PD-relevant deficits. Second, VPS35 expression in DA neurons is necessary for mitochondrial fusion and function, an event critical for DA neuron survival. Third, VPS35 regulates the trafficking and degradation of the E3 ubiquitin ligase MUL1, thus suppressing MUL1-mediated MFN2 degradation, and promotes mitochondrial fusion. Fourth, elevated MUL1 in VPS35-deficient DA neurons contributes to MFN2 reduction, mitochondrial fragmentation, and DA neuron loss, but not to the accumulation of α-synuclein. Our work thus provides evidence for VPS35/retromer's unrecognized function in regulating mitochondrial fusion dynamics, and it suggests a working model in which dysregulation of VPS35/retromer's function results in an increase of mitochondrial MUL1 E3 ubiquitin ligase, a decrease in MFN2, and an impairment of mitochondrial fusion and function, which may underlie VPS35 deficiency/mutation-associated PD pathogenesis.

The dysfunction of VPS35/retromer is believed to be a risk factor for the pathogenesis of both AD and PD. Whereas VPS35 deficiency enhances AD neuropathology in the Tg2576 mouse model of AD (Wen et al., 2011), it was unclear if VPS35 deficiency contributes to PD pathogenesis. Here we provide evidence for VPS35 deficiency or mutation to promote PD pathogenesis. First, $VPS35^{+/-}$ mice exhibit age-dependent PD-like deficit, including TH^+ DA neuron loss and an accumulation of α-synuclein (Tang et al., 2015). Second, young adult $VPS35^{DAT\text{-}Cre}$ mice, which specifically delete the VPS35 gene in DA neurons (Figure S1), show an earlier onset PD-like deficit than $VPS35^{+/-}$ mice (Figure 1), revealing a genetic dose dependency and the importance of VPS35 expression in DA neurons. Third, DA neurons expressing VPS35-D620N (a PD-linked mutation, via AAV virus) also exhibited a reduction in TH^+ neurons (Figure S7).

How does VPS35 deficiency or mutation in DA neurons promote PD pathogenesis? The underlying mechanisms may be complex, as VPS35/retromer regulates the function and trafficking of numerous cargos (Small and Petsko, 2015). Here, we propose that dysfunction in mitochondrial fusion dynamics may be a critical mechanism underlying VPS35 deficiency- or mutation-associated PD pathogenesis for the following reasons. First, the MFN2 protein, a GTPase essential for mitochondrial fusion, was decreased in both $VPS35^{+/-}$ and $VPS35^{DAT\text{-}Cre}$ VM and in VPS35-deficient primary DA neurons (Figure 2), which correlates well with the mitochondrial deficit. Second, expression of VPS35-WT, but not the PD-linked mutant D620N, in VPS35-deficient cells was capable of restoring the phenotypes (such as MFN2 reduction and mitochondrial fragmentation; Figures 3 and 5). Third, DA neuron-selective MFN2 knockout mice ($MFN2^{-/-}$ or $MFN2^{DAT\text{-}Cre}$) showed mitochondrial and PD-relevant deficits (Lee et al., 2012b; Pham et al., 2012). Fourth, MFN2 is mutated in human axonal degenerative disorder Charcot-Marie-Tooth type 2A (Züchner et al., 2004), and MFN2 loss is implicated in the pathogenesis of not only Charcot-Marie-Tooth type 2A but also PD. Finally, the dysregulation of mitochondrial function has been linked to the pathogenesis of multiple neurodegenerative disorders, and the evidence in PD is particularly strong (Haelterman et al., 2014). Mutations in several genes identified in PD patients encode proteins critical for mitochondrial dynamics as well as quality control. Among these genes, α-synuclein, Pink1, Parkin, and DJ-1, their functions on mitochondrial dynamics have been investigated extensively. Although their functions in regulating mitochondrial fusion or fission dynamics remain controversial, studies from *Drosophila*, mouse, and human cell lines support the view for the critical roles that these genes play in maintaining mitochondrial morphology, function, and mitophage-mediated clearance of damaged mitochondria in PD (Lee et al., 2012a; Pickrell and Youle, 2015).

VPS35 is a well-recognized key component of the retromer essential for endosome-to-Golgi retrieval of transmembrane proteins/cargos. This study suggests a crucial role for VPS35 in regulating mitochondrial fusion dynamics, raising a question of how VPS35/retromer, a critical endosomal pathway regulator, regulates MFN2 protein degradation and mitochondrial protein trafficking. Results in our cellular and in vivo mouse studies have led to a working model, in which VPS35 promotes mitochondrial fusion dynamics by increasing MUL1 E3 ubiquitin ligase degradation and suppressing MUL1 mitochondrial targeting, thus preventing MUL1-mediated MFN2 ubiquitination and degradation. This VPS35-MUL1-MFN2 pathway is in line with the reports that MUL1/MAPL promotes ubiquitination and degradation of MFN2 and enhances mitochondrial fission (Braschi et al., 2009; Lokireddy et al., 2012). It is also in agreement with the observations that VPS35 interacts with MUL1/MAPL and is required for the formation of MUL1/MAPL-associated mitochondrial-derived vesicles (MDVs) or MUL1/MAPL-containing peroxisomes in the MCF7 tumor cell line (Braschi et al., 2010). While this model is

supported by both in vitro and in vivo evidence, it is intriguing and raises additional questions. How does VPS35 regulate MUL1/MAPL degradation? Are the sorting nexins and other retromer complex proteins (e.g., Vps26 and 29) involved in this event? Does MUL1/MAPL-mediated Drp1 sumoylation also contribute to the mitochondrial deficit in VPS35-deficient cells/brain? Addressing these questions in future studies may reveal further insights into VPS35/retromer regulation of mitochondrial fusion/fission dynamics and PD pathogenesis.

Notice that altered mitochondrial morphology or fusion dynamics were not only detected in VPS35-deficient DA neurons, but also in VPS35-depleted neuroblastoma cell lines. These results suggest that VPS35 may be a general regulator for mitochondrial fusion dynamics in vitro. However, in vivo/in VPS35$^{+/-}$ brain, dysfunctional mitochondria appeared to be brain region selective and age dependent, mainly detected in PD-vulnerable brain regions, such as SNpc and STR (Figure S4). Consistently, the MUL1 increase and MFN2 reduction in VPS35-deficient mice were also brain region selective, having been detected in SNpc and STR, but not HIP (Figures 2 and 5). These observations suggest a brain region-specific factor that also may regulate MUL1 degradation and mitochondrial function. This factor may be higher in the HIP, but lower in the SNpc and STR. Alternatively, additional factor(s) that occur in VPS35-deficient midbrain lower the threshold to tolerate VPS35/retromer dysfunction in DA neurons as compared to that in other types of neurons, which may contribute to the different results between in vitro and in vivo experiments.

In aggregate, this study provides evidence that loss of VPS35 function in DA neurons results in impaired MUL1 trafficking and degradation and increased MUL1, thus promoting MFN2 degradation, mitochondrial fusion and function impairments, and dopaminergic neuronal loss.

EXPERIMENTAL PROCEDURES

Animals

Two types of VPS35-deficient mice were generated and used in this study. First, VPS35$^{+/-}$ mice were described previously (Wen et al., 2011). Second, VPS35$^{DAT\text{-}Cre}$ mice were generated by crossing floxed allele of VPS35 (VPS35$^{f/f}$) with DAT-Cre mice. The VPS35$^{f/f}$ mice were generated as described in the Supplemental Experimental Procedures. All the mice were backcrossed with C57BL/6 mice for more than six to ten generations. All the mice were housed in a room with a 12-hr light/dark cycle with water and standard rodent chow diet. All the experimental procedures were approved by the Institutional Animal Care and Use Committee at Georgia Regents University.

Stereological Analysis

To quantify the number of DA (TH$^+$) or NeuN$^+$ neurons in SNpc, the unbiased stereological estimation of the total number of the TH$^+$/NeuN$^+$ cells in VM was employed as previously described (Yin et al., 2013). In brief, every fifth section from the bregma −2.92 to −4.16-mm coronal sections across the midbrain was stained with TH/NeuN antibody. The total number of TH$^+$/NeuN$^+$ neurons in each section of SNpc was mathematically calculated using the Stereo Investigator program.

Primary Culture and Transfection

Dopaminergic neuronal culture was prepared as previously described (Lin et al., 2012). Briefly, individual VM of embryonic day (E)18.5 VPS35$^{f/f}$ or VPS35$^{+/m}$ mice was dissected and placed in cold Hank's balanced salt solution (HBSS). The brain pieces were then digested in papain (5 U/ml, Worthington Biochemical) for 20 min at 37°C. Cells were dissociated using increasingly smaller pipette tips, washed twice, resuspended in the plating medium (80% Neurobasal-A and 20% fetal bovine serum), and plated onto poly-D-lysine-coated coverslips at a density of 130,000 cells/well (24-well plate). The growth media supplemented with 1× B27, 2 mM GlutaMAX-1, and 1% penicillin/streptomycin were replaced 4 hr later. At 6 days in vitro (DIV), neurons were subjected to transient transfection by using the calcium phosphate-mediated gene transfer method, as previously described (Zhu et al., 2007).

OCR Measurement

OCR was analyzed in an X96 Extracellular Flux Analyzer with XF Cell Mito Stress test kit (Seahorse Biosciences) at 37°C. DA neurons were plated on poly-D-lysine-coated XF96 cell culture plate at 40,000 per well and cultured for 7 days with 80 μl neuronal culture medium/well. Four wells without neuron seeding from each plate were set as temperature and background control. For measurement, neurons were rinsed gently with 100 μl/well assay medium (XF Base medium [Seahorse Biosciences] with 2 mM glutamine and 10 mM glucose), put into 175 μl/well fresh assay medium, and assayed. Three baseline recordings were made, followed by sequential injection of the ATP synthase inhibitor oligomycin, the mitochondrial uncoupler FCCP, and the complex I inhibitor rotenone. Two-minute OCR measurements were performed at 3-min intervals with mixing, and each condition was measured in an independent well.

Measurement of Mitochondrial Membrane Potential

Mitochondrial membrane potential ($\Delta\Psi$m) was measured with a cationic fluorescent dye, TMRM$^+$ (Molecular Probes). Briefly, NLT cells were transfected with miR-scramble or miR-VPS35 on poly-D-lysine-coated coverslips, and, 48 hr post-transfection, cells were washed and incubated with TMRM$^+$ at 10 nM for 30 min in a Dulbecco's PBS (D-PBS, HyClone). After treatment, cells were imaged at an excitation wavelength of 555 nm and emission wavelength of 580 nm by the fluorescence microscope (Olympus IX70) and captured every 60 s with a 60× objective (Olympus); further analysis of TMRM fluorescence was performed using Image-Pro Plus software.

AAV Generation and Injection

Adenovirus 5 carrying shRNA against mouse-MUL1 (AAV-shR-MUL1) was generated at the Emory virus core facility. The shR-MUL1 (5′- GAGCTGTGC GGTCTGTTAA-3′) was synthetized and subcloned into a pAAV-U6-GFP expression vector (Cell Biolabs). The eGFP cDNA was used as a control after sub-cloning into pAAV-MCS vector (Cell Biolabs). The full length of mouse VPS35-D620N cDNA was sub-cloned into the pAAV-EGFP-T2A-V5 vector (Vector Biolabs). Infected 293 cells from 25–50 15-cm tissue culture plates were collected and centrifuged. Then the cells were lysed by three freeze/thaw cycles. The AAV virus was purified using the iodixanol gradient centrifugation procedure and the virus titers were measured by real-time PCR. For stereotaxic injection, 1.5 μl viral solution (1 × 10^{12} vg/ml) was injected into the right VM (anterior, −2.8 mm; lateral, −1.3 mm; dorsal, −4.2 mm relative to bregma) with a 30-gauge microsyringe at a rate of 0.5 μl/min.

Statistical Analysis

Data were analyzed with Prism 5.0 software (GraphPad). Student's t test and one-way ANOVA with Bonferroni post hoc test were used as indicated. Significance was defined as $p < 0.05$.

SUPPLEMENTAL INFORMATION

Supplemental Information includes Supplemental Experimental Procedures and seven figures and can be found with this article online at http://dx.doi.org/10.1016/j.celrep.2015.08.001.

AUTHOR CONTRIBUTIONS

F.-L.T. and W.-C.X. designed research. F.-L.T. conducted all experiments and data analysis. W.L. performed immunostaining analysis. J.-X.H. prepared AAV vectors for viral injection. J.R.E. performed the behavioral tests. F.-L.T., J.Y.,

L.M., and W.-C.X. discussed the results. F.-L.T. and W.-C.X. wrote the manuscript.

ACKNOWLEDGMENTS

We thank Drs. Xiaoxi Zhuang (University of Chicago), Philip Wang (Georgia Regents University), and Gia Voeltz (University of Colorado) for reagents. We also thank Ms. Shan Xiong for VPS35 mutant mouse maintenance and genotyping, and members of the W.-C.X. and L.M. laboratories for helpful discussions. This study was supported in part by grants from the NIH (AG045781 to W.-C.X.) and Department of Veterans Affairs (BX00838 to W.-C.X.).

Received: August 12, 2014
Revised: July 9, 2015
Accepted: July 31, 2015
Published: August 27, 2015

REFERENCES

Braschi, E., Zunino, R., and McBride, H.M. (2009). MAPL is a new mitochondrial SUMO E3 ligase that regulates mitochondrial fission. EMBO Rep. *10*, 748–754.

Braschi, E., Goyon, V., Zunino, R., Mohanty, A., Xu, L., and McBride, H.M. (2010). Vps35 mediates vesicle transport between the mitochondria and peroxisomes. Curr. Biol. *20*, 1310–1315.

Chan, D.C. (2006a). Dissecting mitochondrial fusion. Dev. Cell *11*, 592–594.

Chan, D.C. (2006b). Mitochondrial fusion and fission in mammals. Annu. Rev. Cell Dev. Biol. *22*, 79–99.

Chen, L.B. (1988). Mitochondrial membrane potential in living cells. Annu. Rev. Cell Biol. *4*, 155–181.

Chen, H., Detmer, S.A., Ewald, A.J., Griffin, E.E., Fraser, S.E., and Chan, D.C. (2003). Mitofusins Mfn1 and Mfn2 coordinately regulate mitochondrial fusion and are essential for embryonic development. J. Cell Biol. *160*, 189–200.

Eaton, S. (2008). Retromer retrieves wntless. Dev. Cell *14*, 4–6.

Gasser, T. (2007). Update on the genetics of Parkinson's disease. Mov. Disord. *22* (*Suppl 17*), S343–S350.

Haelterman, N.A., Yoon, W.H., Sandoval, H., Jaiswal, M., Shulman, J.M., and Bellen, H.J. (2014). A mitocentric view of Parkinson's disease. Annu. Rev. Neurosci. *37*, 137–159.

Itoh, K., Nakamura, K., Iijima, M., and Sesaki, H. (2013). Mitochondrial dynamics in neurodegeneration. Trends Cell Biol. *23*, 64–71.

Karbowski, M., and Youle, R.J. (2003). Dynamics of mitochondrial morphology in healthy cells and during apoptosis. Cell Death Differ. *10*, 870–880.

Knott, A.B., Perkins, G., Schwarzenbacher, R., and Bossy-Wetzel, E. (2008). Mitochondrial fragmentation in neurodegeneration. Nat. Rev. Neurosci. *9*, 505–518.

Lee, Y., Dawson, V.L., and Dawson, T.M. (2012a). Animal models of Parkinson's disease: vertebrate genetics. Cold Spring Harb. Perspect. Med. *2*, a009324.

Lee, S., Sterky, F.H., Mourier, A., Terzioglu, M., Cullheim, S., Olson, L., and Larsson, N.G. (2012b). Mitofusin 2 is necessary for striatal axonal projections of midbrain dopamine neurons. Hum. Mol. Genet. *21*, 4827–4835.

Lin, X., Parisiadou, L., Sgobio, C., Liu, G., Yu, J., Sun, L., Shim, H., Gu, X.L., Luo, J., Long, C.X., et al. (2012). Conditional expression of Parkinson's disease-related mutant α-synuclein in the midbrain dopaminergic neurons causes progressive neurodegeneration and degradation of transcription factor nuclear receptor related 1. J. Neurosci. *32*, 9248–9264.

Lokireddy, S., Wijesoma, I.W., Teng, S., Bonala, S., Gluckman, P.D., McFarlane, C., Sharma, M., and Kambadur, R. (2012). The ubiquitin ligase Mul1 induces mitophagy in skeletal muscle in response to muscle-wasting stimuli. Cell Metab. *16*, 613–624.

Losón, O.C., Song, Z., Chen, H., and Chan, D.C. (2013). Fis1, Mff, MiD49, and MiD51 mediate Drp1 recruitment in mitochondrial fission. Mol. Biol. Cell *24*, 659–667.

MacLeod, D.A., Rhinn, H., Kuwahara, T., Zolin, A., Di Paolo, G., McCabe, B.D., Marder, K.S., Honig, L.S., Clark, L.N., Small, S.A., and Abeliovich, A. (2013). RAB7L1 interacts with LRRK2 to modify intraneuronal protein sorting and Parkinson's disease risk. Neuron *77*, 425–439.

Martin, I., Dawson, V.L., and Dawson, T.M. (2011). Recent advances in the genetics of Parkinson's disease. Annu. Rev. Genomics Hum. Genet. *12*, 301–325.

Muhammad, A., Flores, I., Zhang, H., Yu, R., Staniszewski, A., Planel, E., Herman, M., Ho, L., Kreber, R., Honig, L.S., et al. (2008). Retromer deficiency observed in Alzheimer's disease causes hippocampal dysfunction, neurodegeneration, and Abeta accumulation. Proc. Natl. Acad. Sci. USA *105*, 7327–7332.

Nielsen, M.S., Gustafsen, C., Madsen, P., Nyengaard, J.R., Hermey, G., Bakke, O., Mari, M., Schu, P., Pohlmann, R., Dennes, A., and Petersen, C.M. (2007). Sorting by the cytoplasmic domain of the amyloid precursor protein binding receptor SorLA. Mol. Cell. Biol. *27*, 6842–6851.

Okamoto, K., and Shaw, J.M. (2005). Mitochondrial morphology and dynamics in yeast and multicellular eukaryotes. Annu. Rev. Genet. *39*, 503–536.

Pham, A.H., Meng, S., Chu, Q.N., and Chan, D.C. (2012). Loss of Mfn2 results in progressive, retrograde degeneration of dopaminergic neurons in the nigrostriatal circuit. Hum. Mol. Genet. *21*, 4817–4826.

Pickrell, A.M., and Youle, R.J. (2015). The roles of PINK1, parkin, and mitochondrial fidelity in Parkinson's disease. Neuron *85*, 257–273.

Savitt, J.M., Dawson, V.L., and Dawson, T.M. (2006). Diagnosis and treatment of Parkinson disease: molecules to medicine. J. Clin. Invest. *116*, 1744–1754.

Seaman, M.N. (2004). Cargo-selective endosomal sorting for retrieval to the Golgi requires retromer. J. Cell Biol. *165*, 111–122.

Seaman, M.N. (2012). The retromer complex - endosomal protein recycling and beyond. J. Cell Sci. *125*, 4693–4702.

Small, S.A., and Petsko, G.A. (2015). Retromer in Alzheimer disease, Parkinson disease and other neurological disorders. Nat. Rev. Neurosci. *16*, 126–132.

Small, S.A., Kent, K., Pierce, A., Leung, C., Kang, M.S., Okada, H., Honig, L., Vonsattel, J.P., and Kim, T.W. (2005). Model-guided microarray implicates the retromer complex in Alzheimer's disease. Ann. Neurol. *58*, 909–919.

Tabuchi, M., Yanatori, I., Kawai, Y., and Kishi, F. (2010). Retromer-mediated direct sorting is required for proper endosomal recycling of the mammalian iron transporter DMT1. J. Cell Sci. *123*, 756–766.

Tanaka, A., Cleland, M.M., Xu, S., Narendra, D.P., Suen, D.F., Karbowski, M., and Youle, R.J. (2010). Proteasome and p97 mediate mitophagy and degradation of mitofusins induced by Parkin. J. Cell Biol. *191*, 1367–1380.

Tang, F.L., Erion, J.R., Tian, Y., Liu, W., Yin, D.M., Ye, J., Tang, B., Mei, L., and Xiong, W.C. (2015). VPS35 in dopamine neurons is required for endosome-to-Golgi retrieval of Lamp2a, a receptor of chaperone-mediated autophagy that is critical for α-synuclein degradation and prevention of pathogenesis of Parkinson's disease. J. Neurosci. *35*, 10613–10628.

Vilariño-Güell, C., Wider, C., Ross, O.A., Dachsel, J.C., Kachergus, J.M., Lincoln, S.J., Soto-Ortolaza, A.I., Cobb, S.A., Wilhoite, G.J., Bacon, J.A., et al. (2011). VPS35 mutations in Parkinson disease. Am. J. Hum. Genet. *89*, 162–167.

von Coelln, R., Thomas, B., Andrabi, S.A., Lim, K.L., Savitt, J.M., Saffary, R., Stirling, W., Bruno, K., Hess, E.J., Lee, M.K., et al. (2006). Inclusion body formation and neurodegeneration are parkin independent in a mouse model of alpha-synucleinopathy. J. Neurosci. *26*, 3685–3696.

Wang, C.L., Tang, F.L., Peng, Y., Shen, C.Y., Mei, L., and Xiong, W.C. (2012). VPS35 regulates developing mouse hippocampal neuronal morphogenesis by promoting retrograde trafficking of BACE1. Biol. Open *1*, 1248–1257.

Wen, L., Tang, F.L., Hong, Y., Luo, S.W., Wang, C.L., He, W., Shen, C., Jung, J.U., Xiong, F., Lee, D.H., et al. (2011). VPS35 haploinsufficiency increases Alzheimer's disease neuropathology. J. Cell Biol. *195*, 765–779.

Westermann, B. (2010). Mitochondrial fusion and fission in cell life and death. Nat. Rev. Mol. Cell Biol. *11*, 872–884.

Westermann, B. (2012). Bioenergetic role of mitochondrial fusion and fission. Biochim. Biophys. Acta *1817*, 1833–1838.

Yin, D.M., Chen, Y.J., Lu, Y.S., Bean, J.C., Sathyamurthy, A., Shen, C., Liu, X., Lin, T.W., Smith, C.A., Xiong, W.C., and Mei, L. (2013). Reversal of behavioral deficits and synaptic dysfunction in mice overexpressing neuregulin 1. Neuron *78*, 644–657.

Zhu, X.J., Wang, C.Z., Dai, P.G., Xie, Y., Song, N.N., Liu, Y., Du, Q.S., Mei, L., Ding, Y.Q., and Xiong, W.C. (2007). Myosin X regulates netrin receptors and functions in axonal path-finding. Nat. Cell Biol. *9*, 184–192.

Zhuang, X., Masson, J., Gingrich, J.A., Rayport, S., and Hen, R. (2005). Targeted gene expression in dopamine and serotonin neurons of the mouse brain. J. Neurosci. Methods *143*, 27–32.

Zimprich, A., Benet-Pagès, A., Struhal, W., Graf, E., Eck, S.H., Offman, M.N., Haubenberger, D., Spielberger, S., Schulte, E.C., Lichtner, P., et al. (2011). A mutation in VPS35, encoding a subunit of the retromer complex, causes late-onset Parkinson disease. Am. J. Hum. Genet. *89*, 168–175.

Züchner, S., Mersiyanova, I.V., Muglia, M., Bissar-Tadmouri, N., Rochelle, J., Dadali, E.L., Zappia, M., Nelis, E., Patitucci, A., Senderek, J., et al. (2004). Mutations in the mitochondrial GTPase mitofusin 2 cause Charcot-Marie-Tooth neuropathy type 2A. Nat. Genet. *36*, 449–451.